*Nuclear Mathematical and Computational Sciences: A Century in Review, A Century Anew*
Gatlinburg, Tennessee, April 6-11, 2003, on CD-ROM, American Nuclear Society, LaGrange Park, IL (2003)

# DEVELOPMENT OF A NEW RESONANCE SELF-SHIELDING METHODOLOGY BASED ON PROBABILITY TABLE INFORMATION

**Alain Hébert**
École Polytechnique de Montréal
C.P. 6079 succ. "Centre-Ville"
Montréal Qc. CANADA H3C 3A7
alain.hebert@polymtl.ca

## ABSTRACT

The paper describes the improvement of the lattice code component related to the resonance self-shielding model, which is responsible for the biggest part of the overall error in a lattice calculation. The proposed self-shielding model is based on a new type of probability tables taking into account negative and positive moments of the resonant cross sections, as proposed in the work of Dr. Pierre Ribon. A new type of correlated 2D probability table is used for the representation of the slowing-down effect in the resolved energy domain. The resulting formalism makes possible a better representation of distributed self-shielding effects.

Finally, a validation is presented where the absorption rates obtained with each of these techniques are compared with exact values obtained using a fine-group elastic slowing-down calculation in the resolved energy domain.

*Key Words*: Lattice calculation, Resonance self-shielding, Probability tables, Neutron slowing-down

## 1. INTRODUCTION

A self-shielding model is required in any lattice code in order to take into account the resonant behaviour of the cross sections with an energy discretization based on a limited number of groups (between 50 and 200). The main problem considered in the resonance self-shielding model is how to use self-shielded cross section and probability table information, as retrieved from the isotopic cross-section library. The final objective is to evaluate $\tilde{\sigma}_{\rho,g}$, the microscopic self-shielded cross section for any reaction $\rho$ in group $g$, which is formally defined as

$$\tilde{\sigma}_{\rho,g} = \mu_g \frac{\int_{u_{g-1}}^{u_g} du\, \sigma_\rho(u)\, \phi(u)}{\int_{u_{g-1}}^{u_g} du\, \phi(u)} = \mu_g \frac{\langle \sigma_\rho \phi \rangle_g}{\langle \phi \rangle_g} \tag{1}$$

where $u$ is the lethargy ($= \ln(E_0/E)$), $u_g$ is the upper lethargy limit of group $g$, $\mu_g$ is the SPH factor obtained from the multigroup equivalence procedure, $\phi(u)$ is the neutron flux inside the resonances and $\sigma_\rho(u)$ is the microscopic cross section for nuclear reaction $\rho$.

The self-shielding phenomenon can be explained from the observation that the cross sections belonging to energy group $g$ may include many resonances. Consequently, both $\sigma_\rho(u)$ and $\phi(u)$ exhibit resonant

behavior with peaks and minima in opposite directions. This phenomenon is correctly treated for resonances located in the unresolved energy domain or in the upper part of the resolved energy domain. At higher energies, the resonance flux is given by the well-known Bondarenko expression as

$$\phi(u) = \frac{\sigma_p + \sigma_{\rm e}}{\sigma(u) + \sigma_{\rm e}} \tag{2}$$

where $\sigma(u)$ is the total microscopic cross section (a resonant quantity), $\sigma_p$ is the potential cross section and $\sigma_{\rm e}$ is a dilution parameter function of the amount of self-shielding ($\sigma_{\rm e} = \infty$ in absence of self-shielding). However, complex phenomenas occurs at lower energies. In this case, the slowing-down kernel is acting over an energy range which is not large with respect of the resonance widths. The Bondarenko flux in Eq. (2) cannot be used.

A research program was initiated to improve the self-shielding representation in the lower part of the resolved energy domain. We propose to use a new self-shielding model based on the theory of probability tables, as introduced by P. Ribon *et al.* in Refs. 1, 2 and 3. A new type of correlated probability table is been used to take into account the slowing-down effects at low energy. The Bondarenko flux expression in Eq. (2) is no longer required. The paper presents preliminary results obtained with this approach in the case of a single resonant isotope distributed over the lattice. The interference effects between overlapping resonances has not yet been treated.

The proposed approach is compatible with any flux solution technique, such as the method of collision probability, the method of characteristics or the $S_n$ method. The CPU ressources required by the proposed approach remains small as compared to a Monte-Carlo or to a fine energy group approach. The new method has been implemented in a development version of the lattice code DRAGON.[4]

## 2. DESCRIPTION OF THE PERFORMED WORK

### 2.1. Definition of the Probability Tables

Probability tables corresponding to the microscopic total cross section $\sigma(u)$ can be defined from the probability density $\Pi(\sigma)$. $\Pi(\sigma)d\sigma$ is the probability for the microscopic total cross section of the resonant isotope, to have a value between $\sigma$ and $\sigma + d\sigma$. An illustration of the probability density is shown in Fig. 1.

Using this definition, any Riemann integral in energy, with a $\sigma$–dependent integrand, can be replaced by an equivalent Lebesgue integral:

$$\frac{1}{\Delta u_g} \int_{u_{g-1}}^{u_g} du\ f\left[\sigma(u)\right] = \int_0^{\max(\sigma)} d\sigma\ \Pi(\sigma)\ f(\sigma) \tag{3}$$

where $\Delta u_g = u_g - u_{g-1}$.

The probability density $\Pi(\sigma)$ is represented by a series of $K$ Dirac distributions centered at discrete values $\sigma_k$ of the microscopic total cross section for the resonant isotope. Each discrete level is called a ***subgroup*** and is also characterized by a discrete weight $\omega_k$. The probability density is written

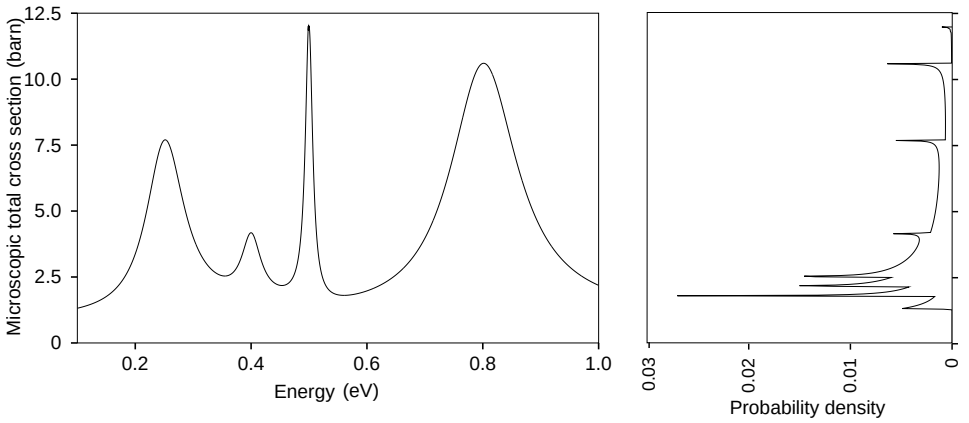


**Figure 1.** Representation of a probability density $\Pi(\sigma)$. The peaks on the right curve are becoming taller with increasing sampling of the left curve.

$$\Pi(\sigma) = \sum_{k=1}^{K} \delta(\sigma - \sigma_k)\, \omega_k \quad . \tag{4}$$

Substitution of Eq. (4) into Eq. (3) leads to the following discretization:

$$\frac{1}{\Delta u_g} \int_{u_{g-1}}^{u_g} du\; f\left[\sigma(u)\right] = \sum_{k=1}^{K} \omega_k\, f(\sigma_k) \quad . \tag{5}$$

The sets of values $\{\omega_k,\ \sigma_k\ ;\ k = 1, K\}$ corresponding to energy group $g$ is called a probability table for the variable $\sigma$.

We also introduce a conditional probability density $\Pi(\sigma, \sigma')$ containing the elastic slowing-down information for the isotope under consideration. $\Pi(\sigma, \sigma')$ is defined in such a way that

$$\frac{1}{(1-\alpha)\Delta u_g} \int_{u_{g-1}}^{u_g} du \int_{u-\epsilon}^{u} du'\, \mathrm{e}^{u'-u}\; f\left[\sigma(u)\right]\; g\left[\sigma(u')\right] = \int_0^{\max(\sigma)} d\sigma \int_0^{\max(\sigma)} d\sigma'\, \Pi(\sigma, \sigma')\, f(\sigma)\, g(\sigma') \tag{6}$$

where $f(\sigma)$ and $g(\sigma)$ are arbitrary functions of the total cross section and where $\epsilon$ is the maximum lethargy jump a neutron can make using an elastic collision with a nucleus of mass ratio $A$ (the ratio of the nucleus mass over the neutron mass). The parameters $\alpha$ and $\epsilon$ are defined as

$$\alpha = \left(\frac{A-1}{A+1}\right)^2 \qquad \text{and} \qquad \epsilon = \ln \frac{1}{\alpha} \quad .$$

As proposed in Ref. 3, the corresponding discretization is written

$$\frac{1}{(1-\alpha)\Delta u_g}\int_{u_{g-1}}^{u_g} du \int_{u-\epsilon}^{u} du' \, \mathrm{e}^{u'-u} \, f\left[\sigma(u)\right] \, g\left[\sigma(u')\right] = \sum_{k=1}^{K}\sum_{\ell=1}^{K} \omega_{k,\ell} \, f(\sigma_k) \, g(\sigma_\ell) \tag{7}$$

where $\omega_{k,\ell}$ is the correlated weight matrix. This matrix is normalized in such a way that

$$\sum_{k=1}^{K} \omega_{k,\ell} = \omega_\ell \qquad \text{and} \qquad \sum_{\ell=1}^{K} \omega_{k,\ell} = \omega_k \quad . \tag{8}$$

Mathematical probability tables are *consistent*: The base points are constrained as follows:

$$\min(\sigma(u)) \leq \sigma_k \leq \max(\sigma(u))$$

the values of the probability table are real, and the weights are positive.

The calculation of a mathematical probability table can be performed using the multiband approach where the base points $\sigma_k$ are known *a priori* or with the CALENDF approach, in which the position of the base points $\sigma_k$ and values of the weights $\omega_k$ are simultaneously determined (see Refs. 2 and 5). Only the CALENDF approach has been investigated.

### 2.2. Calculation of the Probability Tables in Total Cross Section

We first give an overview of the Ribon method, as described in Ref. 5. This method allows the calculation of a probability table for the total cross section in an energy group $g$, using a straightforward transformation of the pointwise information available in the PENDF file.

Negative and positive moments of the total cross section are first computed using

$$\mathcal{M}_\ell = \frac{1}{\Delta u_g}\int_{u_{g-1}}^{u_g} du \, \sigma(u)^\ell \quad . \tag{9}$$

A $K$–order probability table must be capable of preserving $2K$ selected moments of Eq. (9):

$$\sum_{k=1}^{K} \omega_k \, (\sigma_k)^\ell = \mathcal{M}_\ell \;\; ; 1-K \leq \ell \leq K \quad . \tag{10}$$

Negative and positive moments help to preserve the correct self-shielded reaction rate at low and high values of the resonant cross section, respectively.

Considering the Stieltjes generating function of total cross-section moments, defined as a dimensionless quantity, we obtain

$$F(z) = \int_0^{\max(\sigma)} d\sigma\ \Pi(\sigma)\ \frac{(z\sigma)^{1-K}}{1-z\sigma} = \sum_{\ell=1-K}^{K} z^\ell\ \mathcal{M}_\ell\ +\ \mathcal{O}(z^{K+1})\ . \tag{11}$$

where $z$ is an arbitrary variable that can be assimilated to the inverse of a feasible dilution value (i.e., $1/\sigma_\mathrm{e}$).

Using a Padé approximation, this equation can be written

$$z^{K-1}\ F(z) = \sum_{\ell=0}^{2K-1} z^\ell\ \mathcal{M}_{\ell-K+1} = \frac{a_0 + a_1\ z + \ldots + a_{K-1}\ z^{K-1}}{b_0 + b_1\ z + \ldots + b_{K-1}\ z^{K-1} + z^K}\quad . \tag{12}$$

We multiply the denominator of Eq. (12) by $F(z)$, as defined in Eq. (11), and identify the coefficients of the power of $z$ which are between $K$ and $2K-1$. The following linear system is obtained:

$$\begin{bmatrix} \mathcal{M}_K & \mathcal{M}_{K-1} & \ldots & \mathcal{M}_1 \\ \mathcal{M}_{K-1} & \mathcal{M}_{K-2} & \ldots & \mathcal{M}_0 \\ \vdots & \vdots & \ddots & \vdots \\ \mathcal{M}_1 & \mathcal{M}_0 & \ldots & \mathcal{M}_{2-K} \end{bmatrix} \begin{bmatrix} b_0 \\ b_1 \\ \vdots \\ b_{K-1} \end{bmatrix} = - \begin{bmatrix} \mathcal{M}_0 \\ \mathcal{M}_{-1} \\ \vdots \\ \mathcal{M}_{1-K} \end{bmatrix}\quad . \tag{13}$$

A $LDL^\top$ factorization of the coefficient matrix is next performed. The denominator of Eq. (12) is the solution of the factorized linear system and the base points of the probability table are the roots of this polynomial:

$$\prod_{k=1}^{K} (z - \sigma_k) = b_0 + b_1\ z + \ldots + b_{K-1}\ z^{K-1} + z^K\quad . \tag{14}$$

The corresponding weights are chosen so as to preserve selected moments of the total cross section, as used in the discretized form of Eq. (9):

$$\mathcal{M}_\ell = \sum_{k=1}^{K} \omega_k\ \sigma_k^\ell\quad . \tag{15}$$

In the proposed approach, we have chosen to preserve exactly the moments in the interval $-K/2 \leq \ell \leq (K-1)/2$. In this case, the weights are the solution of the following linear system:

$$\begin{bmatrix} 1 & 1 & \ldots & 1 \\ \sigma_1 & \sigma_2 & \ldots & \sigma_K \\ \vdots & \vdots & \ddots & \vdots \\ \sigma_1^{K-1} & \sigma_2^{K-1} & \ldots & \sigma_K^{K-1} \end{bmatrix} \begin{bmatrix} \omega_1\ (\sigma_1)^{k_0} \\ \omega_2\ (\sigma_2)^{k_0} \\ \vdots \\ \omega_K\ (\sigma_K)^{k_0} \end{bmatrix} = \begin{bmatrix} \mathcal{M}_{k_0} \\ \mathcal{M}_{k_0+1} \\ \vdots \\ \mathcal{M}_{k_1} \end{bmatrix} \tag{16}$$

where $k_0 = -K/2$ and $k_1 = (K-1)/2$.

This linear system can be solved without pivoting, using the known analytical inverse of a Vandermonde matrix.[5] We obtain:

$$\omega_k = \frac{(-1)^{K-1}\ (\sigma_k)^{-k_0}}{\prod_{\substack{\ell=1\\ \ell\neq k}}^{K} (\sigma_\ell - \sigma_k)} \sum_{\ell=0}^{K-1} c_{k,\ell}\ \mathcal{M}_{k_0+\ell} \tag{17}$$

where $1 \leq k \leq K$ and where $c_{k,\ell}$ is a coefficient of the polynomial written as

$$c_{k,0} + c_{k,1}\ z + \ldots + c_{k,K-1}\ z^{K-1} = \prod_{\substack{\ell=1\\ \ell\neq k}}^{K} (z - \sigma_\ell) \quad . \tag{18}$$

We will now describe the strategy used to implement this new formalism. For each resonant isotope and each resonant energy group, the probability tables corresponding to different order $K$ are obtained and their accuracy is evaluated by computing Bondarenko self-shielded cross sections for a grid of selected dilutions. The table with smallest order, meeting the accuracy criteria, or the most accurate table, is selected. A maximum order of 12 is allowed, but this order is seldom reached. There is no practical incentive to allow a greater maximum order as high order tables may induce numerical instabilities, overcoming potential increases in accuracy.

### 2.3. The Subgroup Balance Equation

We will first consider the case of an homogeneous mixture made of a unique resonant isotope with other non resonant isotopes. Taking into account the slowing-down effects, the Bondarenko Eq. (2) is replaced with the following expression:

$$\mathbf{r}\{\phi(u)\} + \sigma_{\rm e} = [\sigma(u) + \sigma_{\rm e}]\ \phi(u) \tag{19}$$

where $\mathbf{r}\{\phi(u)\}$ is the microscopic elastic slowing-down operator defined as

$$\mathbf{r}\{\phi(u)\} = \frac{1}{1-\alpha} \int_{u-\epsilon}^{u} du'\ \exp^{-(u-u')}\, \sigma_{\rm s}(u')\ \phi(u') \tag{20}$$

and where $\sigma_{\rm s}(u)$ is the microscopic elastic scattering cross section for the resonant isotope. Note that Eq. (19) is a model, more accurate that the Bondarenko equation, but still neglecting some physical phenomena such as non-elastic resonance scattering and non-uniform distributed source from fission neutrons. Other effects, such as temperature effects, resonance absorption and elastic scattering are accurately taken into account.

Taking the average of Eq. (19) over en energy group $g$, we obtain:

$$\frac{1}{(1-\alpha)\Delta u_g}\int_{u_{g-1}}^{u_g} du \int_{u-\epsilon}^{u} du' \ \exp^{-(u-u')}\ \frac{\sigma_{\rm s}(u')\ \phi(u')}{\sigma(u)+\sigma_{\rm e}} + \frac{1}{\Delta u_g}\int_{u_{g-1}}^{u_g} du\ \frac{\sigma_{\rm e}}{\sigma(u)+\sigma_{\rm e}} = \frac{1}{\Delta u_g}\int_{u_{g-1}}^{u_g} du\ \phi(u) \quad . \tag{21}$$

The flux average is next expressed using the following quadrature:

$$\frac{1}{\Delta u_g}\int_{u_{g-1}}^{u_g} du\ \phi(u) = \sum_{k=1}^{K} \omega_k\ \phi_k \quad . \tag{22}$$

The discretized form of Eq. (21) is therefore written

$$\sum_{k=1}^{K}\sum_{\ell=1}^{K} \omega_{k,\ell}\ \frac{\sigma_{{\rm w},\ell}\ \phi_\ell}{\sigma_k+\sigma_{\rm e}} + \sum_{k=1}^{K} \omega_k\ \frac{\sigma_{\rm e}}{\sigma_k+\sigma_{\rm e}} = \sum_{k=1}^{K} \omega_k\ \phi_k \tag{23}$$

so that

$$\phi_k = \frac{\sigma_{\rm e}}{\sigma_k+\sigma_{\rm e}} + \sum_{\ell=1}^{K} \frac{\omega_{k,\ell}}{\omega_k}\ \frac{\sigma_{{\rm w},\ell}\ \phi_\ell}{\sigma_k+\sigma_{\rm e}} \quad . \tag{24}$$

Eq. (24) is the *subgroup balance equation.* It can be solved to obtain the value of the flux $\phi_k$ in subgroup $k$. The components $\sigma_{{\rm w},k}$ are the base points of the *secondary scattering reaction.* A few steps are required to define this reaction. We first rewrite Eq. (21) as:

$$\frac{1}{(1-\alpha)\Delta u_g}\int_{u_{g-1}}^{u_g} du \int_{u-\epsilon}^{u} du' \ \exp^{-(u-u')}\ \sigma_{\rm s}(u')\ \phi(u') + \sigma_{\rm e} = \frac{1}{\Delta u_g}\int_{u_{g-1}}^{u_g} du\ \phi(u)\,(\sigma(u)+\sigma_{\rm e}) \ . \tag{25}$$

This last equation can be written in term of NJOY–tabulated data as

$$\tau_{\rm w}(\sigma_{\rm e}) + \sigma_{\rm e} = \phi_g(\sigma_{\rm e})\,(\sigma_g(\sigma_{\rm e})+\sigma_{\rm e}) \ . \tag{26}$$

where $\tau_{\rm w}(\sigma_{\rm e})$ is the secondary scattering reaction rate:

$$\tau_{\rm w}(\sigma_{\rm e}) = \sigma_{{\rm w},g}(\sigma_{\rm e})\ \phi_g(\sigma_{\rm e}) = \frac{1}{\Delta u_g}\sum_{h=1}^{G} \Delta u_h\ \sigma_{{\rm s},g\leftarrow h}(\sigma_{\rm e})\ \phi_h(\sigma_{\rm e}) \tag{27}$$

where $G$ is the total number of energy groups.

In the statistical case, we have $\sigma_{\mathrm{w},k} = \sigma_{\mathrm{s},k}$ and $\omega_{k,\ell} = \omega_k\ \omega_\ell$. Eq. (24) simplify to the statistical expression of the subgroup flux:

$$\phi_k = \frac{\sum_{\ell=1}^{K} \omega_\ell\ \sigma_{\mathrm{s},\ell}\ \phi_\ell + \sigma_{\mathrm{e}}}{\sigma_k + \sigma_{\mathrm{e}}} \quad . \tag{28}$$

This last expression has a domain of validity greater than the Bondarenko expression. However, it cannot be used in the lower part of the resolved energy domain where approximation $\omega_{k,\ell} = \omega_k\ \omega_\ell$ is not valid.

Similarly, the *wide resonance* (WR) approximation is set using $\sigma_{\mathrm{w},k} = \sigma_{\mathrm{s},k}$ and $\omega_{k,\ell} = \omega_k\ \delta_{k,\ell}$. Eq. (24) simplify to the WR expression of the subgroup flux:

$$\phi_k = \frac{\sigma_{\mathrm{e}}}{(\sigma_k - \sigma_{\mathrm{s,k}}) + \sigma_{\mathrm{e}}} \quad . \tag{29}$$

The WR approximation can be used on the 6.7eV resonance of $^{238}U$ for medium-accuracy calculations. In the present study, we propose to avoid both ST and WR approximations in the low-energy part of the resolved energy domain and to take into account the slowing-down effects.

### 2.4. Calculation of the Correlated Probability Tables

We now give an overview of the numerical approach used to obtain the correlated base points $\phi_k$, $\sigma_{\mathrm{w},k}$ and $\omega_{k,\ell}$ introduced in the last section. We first obtain the fine group solution of the flux Eq. (19) for a grid of dilution values. Typically, we use the same grid as NJOY. For $^{238}U$, we selected a set of finite dilutions between 1.5 barn and 10000.0 barn containing $L = 18$ values equally spaced on a logarithmic scale.

Negative and positive moments of each fine flux solution are computed using

$$\mathcal{F}_\ell(\sigma_{\mathrm{e}}) = \frac{1}{\Delta u_g} \int_{u_{g-1}}^{u_g} du\ \phi(u, \sigma_{\mathrm{e}})\ \sigma(u)^\ell \quad . \tag{30}$$

A $K$–order probability table must be capable of preserving $K$ selected moments of Eq. (30):

$$\sum_{k=1}^{K} \omega_k\ \phi_k(\sigma_{\mathrm{e}})\ \sigma_k^\ell = \mathcal{F}_\ell(\sigma_{\mathrm{e}})\ \ ; -K/2 \leq \ell \leq (K-1)/2 \quad . \tag{31}$$

This linear system can be written

$$\begin{bmatrix} 1 & 1 & \dots & 1 \\ \sigma_1 & \sigma_2 & \dots & \sigma_K \\ \vdots & \vdots & \ddots & \vdots \\ \sigma_1^{K-1} & \sigma_2^{K-1} & \dots & \sigma_K^{K-1} \end{bmatrix} \begin{bmatrix} \omega_1\ (\sigma_1)^{k_0}\ \phi_1(\sigma_{\mathrm{e}}) \\ \omega_2\ (\sigma_2)^{k_0}\ \phi_2(\sigma_{\mathrm{e}}) \\ \vdots \\ \omega_K\ (\sigma_K)^{k_0}\ \phi_K(\sigma_{\mathrm{e}}) \end{bmatrix} = \begin{bmatrix} \mathcal{F}_{k_0}(\sigma_{\mathrm{e}}) \\ \mathcal{F}_{k_0+1}(\sigma_{\mathrm{e}}) \\ \vdots \\ \mathcal{F}_{k_1}(\sigma_{\mathrm{e}}) \end{bmatrix} \tag{32}$$

where $k_0 = -K/2$ and $k_1 = (K-1)/2$. This linear system can be solved without pivoting, using the known analytical inverse of a Vandermonde matrix.[5] We obtain:

$$\phi_k(\sigma_\mathrm{e}) = \frac{1}{\omega_k} \frac{(-1)^{K-1}\,(\sigma_k)^{-k_0}}{\prod\limits_{\substack{\ell=1 \\ \ell\neq k}}^{K} (\sigma_\ell - \sigma_k)} \sum_{\ell=0}^{K-1} c_{k,\ell}\, \mathcal{F}_{k_0+\ell}(\sigma_\mathrm{e}) \tag{33}$$

where $1 \leq k \leq K$ and where $c_{k,\ell}$ is a coefficient of the polynomial defined in Eq. (18). We assume that the number $L$ of finite dilution values is chosen such that $L+1 \geq K$.

The flux-related base points are organized in the following $(L+1 \times K)$ rectangular matrix:

$$\mathbf{F} = \begin{bmatrix} \phi_1(\sigma_{\mathrm{e},1}) & \phi_2(\sigma_{\mathrm{e},1}) & \dots & \phi_K(\sigma_{\mathrm{e},1}) \\ \phi_1(\sigma_{\mathrm{e},2}) & \phi_2(\sigma_{\mathrm{e},2}) & \dots & \phi_K(\sigma_{\mathrm{e},2}) \\ \vdots & \vdots & \ddots & \vdots \\ \phi_1(\sigma_{\mathrm{e},L}) & \phi_2(\sigma_{\mathrm{e},L}) & \dots & \phi_K(\sigma_{\mathrm{e},L}) \\ 1 & 1 & \dots & 1 \end{bmatrix} \quad . \tag{34}$$

This matrix is factorized according to the $QR$ algorithm described in Ref. 6. We obtain

$$\mathbf{F} = \mathbf{QR} = \mathbf{Q} \begin{bmatrix} \mathbf{R}_1 \\ \mathbf{0} \end{bmatrix} \tag{35}$$

where $\mathbf{Q}$ is a $(L+1 \times L+1)$ orthogonal matrix and $\mathbf{R}_1$ is a $(K \times K)$ upper triangular matrix. The root mean square (RMS) solution of any linear system of the form

$$\mathbf{F}\vec{x} = \vec{\tau} \tag{36}$$

is given as

$$\mathbf{R}\vec{x} = \mathbf{Q}^\top \vec{\tau} = \vec{y} \tag{37}$$

which can be solved by back substitution, using the first $K$ values of vector $\vec{y}$. The same solution could have been obtained from the normal matrix as $\vec{x} = \left(\mathbf{F}^\top\mathbf{F}\right)^{-1}\mathbf{F}^\top\vec{\tau}$. However, the inversion of matrix $\mathbf{F}^\top\mathbf{F}$ is prone to numerical instabilities as its condition number is the square of that of matrix $\mathbf{F}$. The Businger-Golub technique is therefore a logical choice to help reducing the error propagation.

The reference reaction rates $\vec{\tau}_\rho = \{\tau_\rho(\sigma_{\mathrm{e},1}), \tau_\rho(\sigma_{\mathrm{e},2}), \dots, \tau_\rho(\sigma_{\mathrm{e},L}), \tau_\rho(\infty)\}$ for a particular reaction $\rho$ in energy group $g$ are obtained from NJOY–tabulated data as

$$\tau_\rho(\sigma_\mathrm{e}) = \sigma_{\rho,g}(\sigma_\mathrm{e})\; \phi_g(\sigma_\mathrm{e}) \tag{38}$$

The corresponding base points $\vec{x}_\rho = \{\omega_1\sigma_{\rho,1}, \omega_2\sigma_{\rho,2}, \dots, \omega_K\sigma_{\rho,K}\}$ are obtained using the previously described RMS technique as

$$\vec{x}_\rho = \left(\mathbf{F}^\top\mathbf{F}\right)^{-1}\mathbf{F}^\top\vec{\tau}_\rho \quad . \tag{39}$$

This operation is repeated for all resonant partial reaction rate, including self-scattering, scattering to neighbour groups, gamma capture, steady-state and delayed fission reactions. Morever, the calculation of the correlated weight matrix requires the knowledge of the base points corresponding to the secondary scattering reaction. These reference reaction rates are defined by Eq. (27) and the corresponding base points $\vec{x}_{\rm w} = \{\omega_1\sigma_{{\rm w},1}, \omega_2\sigma_{{\rm w},2}, \ldots, \omega_K\sigma_{{\rm w},K}\}$ are obtained by a relation similar to Eq. (39).

The last step is to compute the correlated weight matrix. Care must be taken to satisfy the normalization conditions in Eq. (8). The flux-related base points are reorganized in the following $(L+1\times K)$ rectangular matrix:

$$\mathbf{F}_2 = \begin{bmatrix} \phi_1(\sigma_{{\rm e},1})\ \sigma_{{\rm w},1} & \phi_2(\sigma_{{\rm e},1})\ \sigma_{{\rm w},2} & \ldots & \phi_K(\sigma_{{\rm e},1})\ \sigma_{{\rm w},K} \\ \phi_1(\sigma_{{\rm e},2})\ \sigma_{{\rm w},1} & \phi_2(\sigma_{{\rm e},2})\ \sigma_{{\rm w},2} & \ldots & \phi_K(\sigma_{{\rm e},2})\ \sigma_{{\rm w},K} \\ \vdots & \vdots & \ddots & \vdots \\ \phi_1(\sigma_{{\rm e},L})\ \sigma_{{\rm w},1} & \phi_2(\sigma_{{\rm e},L})\ \sigma_{{\rm w},2} & \ldots & \phi_K(\sigma_{{\rm e},L})\ \sigma_{{\rm w},K} \\ 1 & 1 & \ldots & 1 \end{bmatrix} \quad . \tag{40}$$

Next, a dilution–dependent normalization factor is computed as

$$f(\sigma_{\rm e}) = \frac{\sum\limits_{k=1}^{K} \omega_k\ \phi_k(\sigma_{\rm e})\ \sigma_{{\rm w},k}}{\sum\limits_{k=1}^{K} \omega_k\ \left[\phi_k(\sigma_{\rm e})\ (\sigma_k+\sigma_{\rm e}) - \sigma_{\rm e}\right]} \quad . \tag{41}$$

The RHS $(L+1\times K)$ coefficient matrix $\mathbf{B}$ is computed as

$$\mathbf{B} = \begin{bmatrix} \beta_1(\sigma_{{\rm e},1}) & \beta_2(\sigma_{{\rm e},1}) & \ldots & \beta_K(\sigma_{{\rm e},1}) \\ \beta_1(\sigma_{{\rm e},2}) & \beta_2(\sigma_{{\rm e},2}) & \ldots & \beta_K(\sigma_{{\rm e},2}) \\ \vdots & \vdots & \ddots & \vdots \\ \beta_1(\sigma_{{\rm e},L}) & \beta_2(\sigma_{{\rm e},L}) & \ldots & \beta_K(\sigma_{{\rm e},L}) \\ \omega_1 & \omega_2 & \ldots & \omega_K \end{bmatrix} \tag{42}$$

where

$$\beta_k(\sigma_{\rm e}) = \omega_k\ \left[\phi_k(\sigma_{\rm e})\ (\sigma_k+\sigma_{\rm e}) - \sigma_{\rm e}\right] f(\sigma_{\rm e}), \quad \text{if } \sigma_{\rm e} \neq \infty \quad . \tag{43}$$

The correlated weight matrix $\mathbf{W}$ can be obtained in term of a normal matrix as

$$\mathbf{W} = \left(\mathbf{F}_2^\top \mathbf{F}_2\right)^{-1} \mathbf{F}_2^\top \mathbf{B} \quad . \tag{44}$$

Again, error propagation can be greatly reduced by performing the $QR$ factorization of matrix $\mathbf{F}_2$ and by using the Businger-Golug technique to directly obtain $\mathbf{W}$ without actually computing the normal matrix.

### 2.5. The Collision Probability Subgroup Equation

We define $\phi_{i,k}$ as the flux in region $i$ and subgroup $k$. The collision probability form of Eq. (24) can be used to describe an heterogeneous case. We obtain

$$\phi_{i,k} = \sum_{j=1}^{I} p_{ij,k} \left( \Sigma^{+}_{\mathrm{s},j} + \sum_{\ell=1}^{K} \frac{\omega_{k,\ell}}{\omega_k} \, \Sigma^{*}_{\mathrm{w},j,\ell} \, \phi_{j,\ell} \right) \quad . \tag{45}$$

where $\Sigma^{+}_{\mathrm{s},j}$ is the macroscopic $P_0$ scattering cross section of the non–resonant isotopes in region $j$ and $\Sigma^{*}_{\mathrm{w},j,\ell}$ is the macroscopic secondary scattering cross section of the resonant isotopes in subgroup $\ell$ and region $j$.

Unfortunately, Eq. (45) cannot be solved using an iterative approach because the correlated weight matrix is not positive definite in highly resonant energy groups. We have therefore chosen a response matrix approach requiring the solution of $I \times K$ flux equations in each energy group. This approach will be described in term of the collision probability method but could be extended to other flux solution techniques such as the method of characteristics or the discrete ordinate method. Note that both ST and WR models introduced in Eqs. (28) and (29) produce positive definite correlated weight matrices and are therefore eligible to an iterative approach. The response matrix approach can therefore be limited to the the low-energy resonant groups where the ST model is unable to take into account the slowing-down effects.

The response matrix approach requires the calculation of the following *response coefficients*:

$$M_{i,k\leftarrow\mathrm{source}} = \sum_{j=1}^{I} p_{ij,k} \, \Sigma^{+}_{\mathrm{s},j} \qquad \text{and} \qquad M_{i,k\leftarrow j,\ell} = p_{ij,k} \, \frac{\omega_{k,\ell}}{\omega_k} \, \Sigma^{*}_{\mathrm{w},j,\ell} \quad . \tag{46}$$

The subgroup flux solution is found by solving the corresponding linear system:

$$\begin{bmatrix} M_{1,1\leftarrow1,1} & M_{1,1\leftarrow2,1} & \cdots & M_{1,1\leftarrow1,2} & M_{1,1\leftarrow2,2} & \cdots \\ M_{2,1\leftarrow1,1} & M_{2,1\leftarrow2,1} & \cdots & M_{2,1\leftarrow1,2} & M_{2,1\leftarrow2,2} & \cdots \\ \vdots & \vdots & \ddots & \vdots & \vdots & \\ M_{1,2\leftarrow1,1} & M_{1,2\leftarrow2,1} & \cdots & M_{1,2\leftarrow1,2} & M_{1,2\leftarrow2,2} & \cdots \\ M_{2,2\leftarrow1,1} & M_{2,2\leftarrow2,1} & \cdots & M_{2,2\leftarrow1,2} & M_{2,2\leftarrow2,2} & \cdots \\ \vdots & \vdots & & \vdots & \vdots & \ddots \end{bmatrix} \begin{bmatrix} \phi_{1,1} \\ \phi_{2,1} \\ \vdots \\ \phi_{1,2} \\ \phi_{2,2} \\ \vdots \end{bmatrix} = \begin{bmatrix} M_{1,1\leftarrow\mathrm{source}} \\ M_{2,1\leftarrow\mathrm{source}} \\ \vdots \\ M_{1,2\leftarrow\mathrm{source}} \\ M_{2,2\leftarrow\mathrm{source}} \\ \vdots \end{bmatrix} \quad . \tag{47}$$

After calculation of the subgroup flux unknowns, it is possible to compute the integrated flux $\langle \phi_i \rangle_g$ and reaction rate $\langle \sigma_{\rho,i} \, \phi_i \rangle_g$ for reaction $\rho$ in region $i$ using

$$\langle \phi_i \rangle_g = \sum_{k=1}^{K} \omega_k \, \phi_{i,k} \quad \text{and} \quad \langle \sigma_{\rho,i} \, \phi_i \rangle_g = \sum_{k=1}^{K} \omega_k \, \sigma_{\rho,i,k} \, \phi_{i,k} \tag{48}$$

where the probability table of group $g$ is been used.

### 2.6. The Multigroup Equivalence Procedure

The direct self-shielded cross section for reaction $\rho$ are obtained by substituting the integrated flux and reaction rate Eq. (48) into Eq. (1) with $\mu_g = 1$. We obtain

$$\bar{\sigma}_{\rho,i,g} = \frac{\langle \sigma_{\rho,i}\ \phi_i \rangle_g}{\langle \phi_i \rangle_g} \quad . \tag{49}$$

These cross sections cannot be used directly in a coarse group calculation, since this type of condensation generally does not permit conservation of the reaction rates.[10] We consequently perform a multigroup equivalence procedure and introduce an SPH corrective factor for each region and coarse energy group and define equivalent cross sections by the relations:

$$\widetilde{\sigma}_{\rho,i,g} = \mu_{i,g}\ \bar{\sigma}_{\rho,i,g} \tag{50}$$

where $\mu_{i,g}$ is the SPH factor assigned to region $i$ in group $g$. Note that the SPH factors are equal to 1 in homogeneous-geometry cases.

We need to compute SPH-corrected cross sections over each region and coarse energy group so as to preserve reference sources $Q_{i,g}$ and interpolated reaction rates in the form $\langle \sigma_{\rho,i}\ \phi_i \rangle_g$. The reference sources $Q_{i,g}$ are defined as a sum of scattering rates in order to be consistent with Eq. (26):

$$Q_{i,g} = \Sigma^{+}_{\mathrm{s},i,g} + \left\langle \Sigma^{*}_{\mathrm{w},i}\ \phi_i \right\rangle_g \tag{51}$$

where $\Sigma^{*}_{\mathrm{w},i}$ is the macroscopic secondary scattering cross section for the resonant isotopes in region $i$.

The same SPH factor should be used to multiply every resonant cross section belonging to each region and coarse energy group. We have chosen not to modify non-resonant cross sections mixed with resonant ones. Moreover, the corresponding integrated flux should be redefined using the relation

$$\widetilde{\phi}_{i,g} = \frac{1}{\mu_{i,g}}\ \phi_{i,g} \quad . \tag{52}$$

There is an intrinsic overdetermination for this type of SPH procedure when it is applied to a closed domain. An infinity of sets $\{\mu_{i,g}\ ;\ i = 1, I\}$ allows the target reaction rates to be preserved. A normalization condition should therefore be applied in each group $g$ to determine a single solution. Here, we chose to preserve the average fine-structure in the non-resonant regions, in order to avoid any modification of the cross sections located in the non-resonant regions. [10] We therefore write

$$\mu_{i,g} = 1 \quad ; \quad \text{if } i \notin \mathcal{F} \tag{53}$$

where $\mathcal{F}$ is the set of resonant (fuel) region indices.

In each energy group $g$, a fixed point iteration is used to compute the SPH factor $\mu_{i,g}$. On iteration $(n)$, the SPH-corrected fine-structure is directly obtained as

$$\tilde{\phi}_{i,g}^{(n)} = \sum_{\substack{j=1 \\ j\in\mathcal{F}}}^{I} \tilde{p}_{ij,g}^{(n-1)}\, Q_{j,g} + \sum_{\substack{j=1 \\ j\notin\mathcal{F}}}^{I} \tilde{p}_{ij,g}^{(n-1)}\, \Sigma_{\mathrm{s},j,g}^{+} \quad ; \quad \text{if } i \in \mathcal{F} \tag{54}$$

where the reduced CPs are computed using total cross sections corrected with the SPH factor of previous iteration $(n-1)$. This fixed point iteration can be accelerated by subtracting the following equation

$$\sum_{\substack{j=1 \\ j\in\mathcal{F}}}^{I} \tilde{p}_{ij,g}^{(n-1)}\, \tilde{\Sigma}_{j,g}^{(n-1)}\, \tilde{\phi}_{j,g}^{(n-1)} = \sum_{\substack{j=1 \\ j\in\mathcal{F}}}^{I} \tilde{p}_{ij,g}^{(n-1)} \left[ \Sigma_{j,g}^{+} \langle \phi_j \rangle_g + \left\langle \Sigma_j^{*}\, \phi_j \right\rangle_g \right] \quad ; \quad \text{if } i \in \mathcal{F} \tag{55}$$

from Eq. (54). Here, $\tilde{\Sigma}_{i,g}^{(n-1)}$ is the SPH-corrected macroscopic total cross section of region $i$ at iteration $(n-1)$. We next define a reduced collision probability matrix as

$$\tilde{\mathbf{W}}_g^{(n-1)} = \left[ \mathbf{I} - \tilde{\mathbf{P}}_g^{(n-1)}\ \tilde{\mathbf{\Sigma}}_g^{(n-1)} \right]^{-1} \tilde{\mathbf{P}}_g^{(n-1)} \tag{56}$$

where $\tilde{\mathbf{P}}_g^{(n-1)} = \{ \tilde{p}_{ij,g}^{(n-1)}\ ;\ \ i = 1, I \ \text{ and } \ j = 1, I \ \}$ and where $\tilde{\mathbf{\Sigma}}_g$ is a diagonal cross section matrix defined as

$$\tilde{\mathbf{\Sigma}}_g^{(n-1)} = \mathrm{diag} \begin{cases} \tilde{\Sigma}_{i,g}^{(n-1)}, & \text{if } i \in \mathcal{F}; \\ 0, & \text{otherwise,} \end{cases}$$

so that Eq. (54) is rewritten as

$$\vec{\Phi}_g^{(n)} = \tilde{\mathbf{W}}_g^{(n-1)}\, \vec{S} \tag{57}$$

where the components of vector $\vec{S}$ are defined as

$$S_i = \begin{cases} Q_{i,g} - \Sigma_{i,g}^{+} \langle \phi_i \rangle_g - \langle \Sigma_i^{*} \phi_i \rangle_g\,, & \text{if } i \in \mathcal{F}; \\ \Sigma_{\mathrm{s},i,g}^{+}, & \text{otherwise.} \end{cases} \tag{58}$$

The improved SPH factor is simply

$$\mu_{i,g}^{(n)} = \frac{\langle \phi_i \rangle_g}{\tilde{\phi}_{i,g}^{(n)}} \quad . \tag{59}$$

The iterative process is carried until convergence. Note that the same quantity $\langle \phi_i \rangle_g$ appears in the denominator of Eq. (49) and in the numerator of Eq. (59). It can therefore be simplified, as only the product of these two equations needs to be computed:

$$\widetilde{\sigma}_{\rho,g} = \frac{\langle \sigma_{\rho,f} \ \phi_i \rangle_g}{\tilde{\phi}_{i,g}^{(n)}} \quad . \tag{60}$$

However, knowledge of $\langle \phi_i \rangle_g$ is useful as an initial estimate of the flux or with the "no-sph" option of the self-shielding operator.

## 3. NUMERICAL RESULTS

Two computer codes have been used to implement this new self-shielding model:

1. A computer code, named CESCOL, makes it possible to solve a fixed-source slowing-down equation using an elastic slowing-down operator for a mixture of heavy (resonant) isotopes in the resolved energy domain.[7] A homogeneous option is available and can be used to produce cross section tabulated data that can be interpolated in dilution. Heterogeneous cases can also be treated using CP techniques and used to generate reference solutions. CESCOL is used to produce both the reference solution and the cross section tabulated data at selected dilutions. We choose a set of dilutions $\sigma_e$ between 1.5 barn and 10000.0 barn containing $L = 18$ finite values equally spaced on a logarithmic scale. Infinite dilution ($1.0 \times 10^{10}$ barns) was also chosen.

2. A self-shielding operator was written in a development version of the DRAGON lattice code[4], based on the subgroup model presented in this paper. Self-shielded cross sections are obtained for a coarse energy grid and used in the existing CP flux solution operators. Consistency is emphasized by using the same CP calculation operator in both heterogeneous CESCOL and lattice code calculations.

The validation tests presented in this study are limited to the resolved energy domain where it is possible to precisely define the resonant cross sections. Cross sections were defined in the resolved energy domain and distributed over APOLLO-1 energy groups 31 to 52, located between 2.7679 and 677.3 eV. A 1.0 n/cm$^3$·s source was placed in group number 31, located between 454 eV and 677.3 eV. We studied the absorption rates for the resonant isotopes in energy groups 33 to 52 and reported the discrepancies between CESCOL and lattice code calculations for a set of four benchmarks, the first three been identical to those of Ref. 7.

1. A pure homogeneous case made of a mixture of $^{238}$U ($2.2 \times 10^{22}$ atom/cc), oxygen ($6.9 \times 10^{22}$ atom/cc) and hydrogen ($5.0 \times 10^{22}$ atom/cc).

**Table I. Isotopic data for Benchmarks 1, 2, 3 and 4[a].**

| Mixture | Isotope | Density ($10^{24}$ atom/cc) | Temperature (K) |
|---|---|---|---|
| 1 | $^{238}$U | $2.2 \times 10^{-2}$ | 973.16 |
| | $^{16}$O | $4.4 \times 10^{-2}$ | |
| 2 | Natural Cr | $1.48 \times 10^{-2}$ | |
| | $^{55}$Mn | $9.0 \times 10^{-4}$ | |
| | Natural Fe | $5.3 \times 10^{-2}$ | |
| | Natural Ni | $6.9 \times 10^{-3}$ | |
| 3 | $^{1}$H | $5.0 \times 10^{-2}$ | |
| | $^{16}$O | $2.5 \times 10^{-2}$ | |

$(a)$ Benchmarks 1 and 2 use only mixtures 1 and 3

2. This Benchmark is a pure two-region cylindrical geometry with radii of 0.4095 and 0.7054 cm. The inner cylinder contains the fuel, a mixture of $^{238}$U ($2.2 \times 10^{22}$ atom/cc) and oxygen ($4.4 \times 10^{22}$ atom/cc) whereas the outer cylinder contains light water ($2.5 \times 10^{22}$ molecule/cc).

3. This heterogeneous Benchmark represents a simplified $5 \times 5$ PWR assembly featuring a water hole surrounded by square and rectangular fuel cells that include cladded fuel rods of different diameters. The fuel, clad and coolant properties are defined in Table I. CPs for this Benchmark were obtained using the EURYDICE-2[8] operator available in both CESCOL and in the lattice code.

4. The fourth Benchmark was set to study the distributed self shielding effects within the fuel rod. The fuel rod is subdivided into six annular volumes and the absorption rate is compute in each subvolume. Two versions of this benchmark were studied, with ($4a$) and without ($4b$) taking into account the distributed self-shielding effects. Version $4b$ is obtained by using the same mixture index in the six annular volumes and is equivalent to the approach used in previous–generation lattice codes.

The absorption rates obtained using our self-shielding model are compared to reference results and a maximum $\epsilon^{\max}$, averaged $\bar{\epsilon}$ and integrated error $\epsilon^{\text{int}}$ are computed for each numerical test. The main purpose of the numerical tests was to compare the proposed self-shielding methodology (identified as "Ribox") with reference CESCOL calculations and with results obtained with competing self-shielding methods, namely,

**the Sanchez-Coste method** This is the production self-shielding method used in APOLLO2.[5,9] This method is based on the same mathematical probability tables as the Ribox approach, without making use of the correlated weight matrix $\omega_{k,\ell}$. Instead, an equivalent dilution is computed and used to interpolate self-shielding information from NJOY-tabulated values.

**the USS method** This is the Universal Self-Shielding (USS) method [10,11] developed over the recent years to replace the Generalized Stamm'ler method actually used in DRAGON.[7] This approach is very similar to the method used in Wims-7[12] and Helios[13].

Both Sanchez-Coste and USS methods use an ST-WR(44) slowing-down model, meaning a statistical slowing-down model for resonant group indices smaller than 44 and a wide resonance slowing-down model for other resonant groups. The corresponding numerical results are presented in Table II. The distribution of the absorption rates is plotted in Fig. 2 for the reference case and for the three self-shielding models. The percent accuracies $\epsilon_i^{\rm int}$ of the absorption rates in each annular volume $i$ are presented in Table III.

**Table II. Summary of Benchmark results.**

| | Ribox | | | | | Sanchez-Coste | | | | | USS | | | | |
|---|---|---|---|---|---|---|---|---|---|---|---|---|---|---|---|
| Benchmark | 1 | 2 | 3 | 4a | 4b | 1 | 2 | 3 | 4a | 4b | 1 | 2 | 3 | 4a | 4b |
| $\epsilon^{\rm int}$ (%) | 0.1 | 0.03 | 0.4 | 0.2 | 1.4 | 0.1 | 0.5 | 0.7 | 0.7 | 1.8 | 0.1 | 0.4 | 0.7 | 1.2 | 1.6 |
| $\bar{\epsilon}$ (%) | 0.3 | 0.4 | 0.5 | 0.7 | 1.1 | 0.3 | 0.4 | 0.7 | 0.8 | 1.4 | 0.3 | 0.5 | 0.7 | 1.2 | 1.4 |
| $\epsilon^{\rm max}$ (%) | 1.1 | 1.4 | 2.8 | 4.5 | 4.2 | 1.1 | 1.5 | 3.2 | 5.1 | 5.0 | 1.1 | 1.5 | 3.2 | 4.7 | 5.1 |
| in group | 49 | 49 | 43 | 43 | 43 | 49 | 43 | 43 | 43 | 40 | 49 | 35 | 43 | 43 | 40 |

**Table III. Distributed Self-Shielding Percent Accuracies in Benchmark 4.**

| | Ribox | | Sanchez-Coste | | USS | |
|---|---|---|---|---|---|---|
| | 4a | 4b | 4a | 4b | 4a | 4b |
| 1 | 0.5 | 39.0 | 0.6 | 39.6 | 1.8 | 39.4 |
| 2 | 0.3 | 24.2 | 0.3 | 24.8 | 1.9 | 24.5 |
| 3 | 0.2 | 6.1 | -0.01 | 6.6 | 2.0 | 6.4 |
| 4 | -0.01 | -14.5 | -0.1 | -14.1 | 1.7 | -14.3 |
| 5 | -0.1 | -40.3 | 0.2 | -40.0 | 0.7 | -40.2 |
| 6 | -0.02 | -67.0 | 2.8 | -66.9 | -1.2 | -67.0 |

We observe that the four curves are almost indistinguishables, with the exception of the curve corresponding to the USS method which shows a constant discrepancy of about 2%. In fact, the most accurate self-shielding model is the Ribox method, with a maximum integrated error of 0.5%.

## 4. CONCLUSIONS

We have succussfully developed a self-shielding method based on the rigorous probability table theory of Dr. P. Ribon. This method is slightly more accurate than the current approaches on four simple multigroup benchmarks. The distributed self-shielding effects are accurately taken into account.

However, more work is required before switching to this new method. We first have to investigate its compatibility with existing cross-section libraries and show its accuracy on the Rowland's Benchmarks.[5,14] Comparisons will be performed between self-shielded reaction rates obtained with the proposed self-shielded model and with a Monte-Carlo Code such as MCNP.[15] These studies will highlight

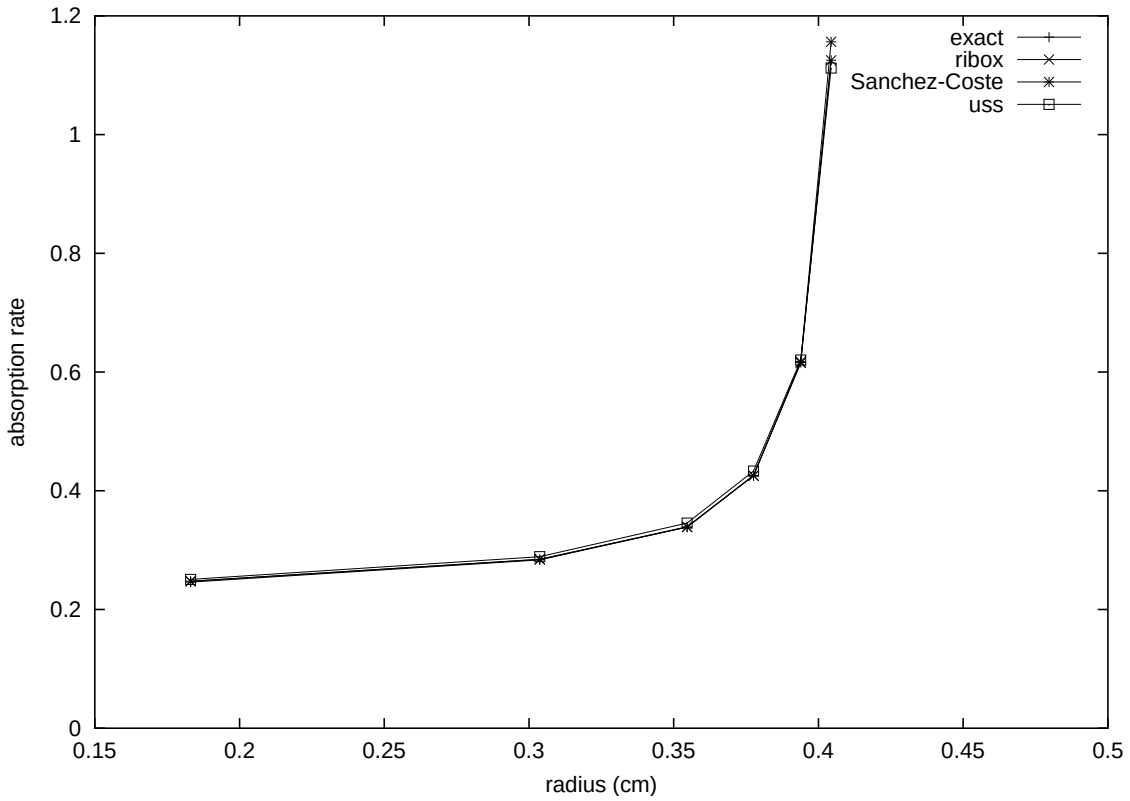


**Figure 2.** Rim effect in a fuel rod for Benchmark 4.

the advantage and drawbacks of using a more complicated self-shielding model. Finally, we have to test its behavior on depletion cases, as the overall reactivity loss between high and low burnup is closely related to the self-shielding accuracy.

## ACKNOWLEDGEMENTS

This work was supported by a grant from the Natural Science and Engineering Research Council of Canada.

## REFERENCES

[1] P. Ribon et J.-M. Maillard, “Les tables de probabilité. Application au traitement des sections efficaces pour la neutronique”, Note CEA–N–2485, Commissariat à l’Énergie Atomique, Juin 1986.

[2] P. Ribon, “Statistical Probability Tables. CALENDF Program,” *Proc. of the Seminar on NJOY and THEMIS*, Saclay, France, June 20-21, 1989, p.220 – 232, OECD/NEA Data Bank (1989).

[3] B. Oum Keltoum Aziza and P. Ribon, “Tables de probabilité non statistiques. Description des effets du ralentissement”, *Proc. Int. Conf. on the Physics of Reactors: Operation, Design and Computation*, Marseille, France, April 23 – 27, 1990.

[4] G. Marleau, A. Hébert and R. Roy, “New Computational Methods Used in the Lattice Code Dragon,” *Proc. Int. Top. Mtg. on Advances in Reactor Physics*, Charleston, USA, March 8-11, 1992.

[5] A. Hébert and M. Coste, “Computing Moment-Based Probability Tables for Self-Shielding Calculations in Lattice Codes”, *Nucl. Sci. Eng.*, **142**, 1 (2002).

[6] P. Businger and G. H. Golub, “Linear Least Square Solutions by Householder Transformations”, *Numerische Mathematik*, **7**, 269 (1965).

[7] A. Hébert and G. Marleau, “Generalization of the Stamm’ler Method for the Self-Shielding of Resonant Isotopes in Arbitrary Geometries,” *Nucl. Sci. Eng.*, **108**, 230 (1991).

[8] A. HÉBERT, “Développement de la methode SPH: Homogénéisation de cellules dans un réseau non uniforme et calcul des paramètres de réflecteur,” CEA- N-2209, Commissariat à L’Énergie Atomique, France (1981).

[9] M. Coste, “Absorption Résonnante des noyaux lourds dans les eéseaux hétérogènes. Formalisme du module d’autoprotection d’APOLLO2””, Note CEA–N–2746, Commissariat à l’Énergie Atomique, Janvier 1994.

[10] A. Hébert, “Advances in the Development of a Subgroup Method for the Self-Shielding of Resonant Isotopes in Arbitrary Geometries”, *Nucl. Sci. Eng.*, **126**, 245 (1997).

[11] A. Hébert, “A Comparison of Three Methods for Computing Probability Tables”, *Proc. Int. Conf. on the Physics of Nuclear Science and Technology*, Hauppage, New York, October 5–8, 1998.

[12] M. J. Halsall, “WIMS7, An Overview,” *Proc. Int. Conf. on the Physics of Reactors – PHYSOR 96*, Mito, Japan, p. B-1, September 16-20 (1996).

[13] J.J. Casal, R.J.J. Stamm’ler, E.A. Villarino and A.A. Ferri “HELIOS: Geometric Capabilities of a New Fuel-Assembly Program,” *Proc. Int. Top. Mtg. on Advances in Mathematics, Computation, and Reactor Physics*, Pittsburgh, Pennsylvania, April 28–May 2, 1991, Vol. 2, p.10.2.1 1–13.

[14] J. ROWLANDS et al, “LWR Pin Cell Benchmark Intercomparisons. An Intercomparison study organized by the JEF Project, with contributions by Britain, France, Germany, The Netherlands, Slovenia and the USA.,” *JEF Report to be published* , OECD/NEA Data Bank (1999).

[15] J. F. Briesmeister, ed., “MCNP– A General Monte Carlo N-Particle Transport Code”, LA-12625-M, Version 4B, March 1997.